Conformation of Polyimide Backbone Structures for Determination of the Pretilt Angle of Liquid Crystals

Yaw-Terng Chern* and Ming-Hung Ju

Department of Chemical Engineering, National Taiwan University of Science and Technology, Taipei, Taiwan, Republic of China

Received October 8, 2008; Revised Manuscript Received November 20, 2008

ABSTRACT: The aromatic polyimides (PIs) containing pendent *tert*-butyl side groups were synthesized via polycondensation of 1-(4-aminophenoxy)-4-(4-aminophenyl)-2,6-di-*tert*-butyl-benzene (**4**), 4-(4-aminophenyl)-1-(4-amino-2-trifluoromethylphenoxy)-2,6-di-*tert*-butyl-benzene with various aromatic tetracarboxylic dianhydrides. The conformation of 2,6-di-*tert*-butyl-1-(4-phthalimidophenoxy)-4-(4-phthalimidophenyl)benzene created the two orthogonally molecular planes. Uniform alignment layers, the three PIs possessing high pretilt angles ranging from 87.9 to 88.7°, have been achieved after mechanical rubbing of the PI thin film surfaces at room temperature and subsequent annealing. This unusual high pretilt angle of PIs containing only short side groups is quite different for most of the typical PIs. The unusual high pretilt angles were predominately governed by their flat-straight conformations. ^{1}H NMR spectrum of the diamine 4 revealed that the protons of 4-aminophenoxy moiety are not chemical shift equivalent. This is because the steric hindrance of the bulky *tert*-butyl groups prevents the benzene ring of the 4-aminophenoxy moiety from rotating freely. These protons produced individual broad singlet signals. These novel PIs exhibited a low dielectric constant (2.75 to 3.11), low moisture absorption (0.65 to 1.74), excellent solubility, and high glass-transition temperatures (337−456 °C). The nonfluorinated PIs derived from the new diamines and the rigid pyromellitic diamhydride (PMDA) were soluble in *N*-methyl-2-pyrrolidinone, *N*,*N*-dimethylacetamide, and *m*-cresol.

Introduction

Aromatic polyimides (PIs) are widely applied in many fields of advanced technology because of their excellence in mechanical and thermal stability. One of the most recently developed and important applications of PIs is their use in liquid crystal (LC) alignment layers due to their outstanding key properties such as thermal stability, high mechanical strength, excellent electrical properties, and so on. One of the key technologies in a liquid crystal display (LCD) is surface alignment of LCs. Mechanically rubbed PI films have been most widely used to align the LC molecules. Much effort has been exerted in understanding the mechanism behind the alignment of LC molecules on the rubbed polymer surface.[1−13] However, the mechanism of alignment has not been completely understood. There are two major models of view: First, periodic microgrooves generated by rubbing may force the LC molecules at the alignment layer surface to be parallel to the rubbing direction because of geometric restrictions between surface microgrooves and LC molecules.[1] Second, an intermolecular interaction between LC molecules and oriented polymers at the alignment layer surface may play a predominant role in aligning LC molecules.[2] As for the previous studies, it is now well recognized that for rubbed polyimide films, the molecular chain reorientation plays a more important role in LC alignment than do microgrooves.[2−13] These results suggest the importance of knowing the molecular orientation and geometric structure of the polyimide surface. Previously, all rubbed PIs had been reported to align LCs along the rubbing direction.[2−13] Interestingly, Nishikawa et al. and Chae et al. found that LCs on a PI surface had been induced to align in the direction perpendicular to the rubbing direction.[4f,9c]

To attain good quality of the LCD devices, many factors should be taken into account such as the viewing angle, optical contrast, response time, and LC alignment stability. However, the pretilt angle plays the most important role in determining the optical and electrical performance of the industrial LCD devices. The conventional PI alignment layer can achieve only a small pretilt angle.[7,12] PIs that induce a high pretilt angle are needed for specially tailored display applications. For example, a vertical alignment method has been used to improve the alignment of the LCs with negative dielectric anisotropy for a faster response time and a higher contrast ratio compared with those of twisted nematic LCDs.[14] Some recent reports have pointed out that alkyl side chains greatly elevate the pretilt angle and that alkyl side-chain PIs could be very promising candidates for excellent LC alignment layers.[4c,7,8b,9d,e,12,15a] As widely reported, the long alkyl side chain with more than 10 carbon atoms is well known for its positive effect on the LC alignment and achievement of a high pretilt angle.[15b] Those materials that induce a high pretilt angle often contain some fluorinated group that tends to stick out of the surface of the PI.[4d,e] One of the most significant scientific ideas is whether high pretilt angle alignment layers can be obtained after rubbing by the introduction of side chains on PI backbones for adjusting the structure and chemical properties.

It was reported that a pretilt angle of LC molecules is mainly affected by van der Waals interactions and the inclination angle of polymer backbones.[4c,15a] In contrast, other investigators reported that the pretilt angles were affected by a geometric structure of the PI film surface, not the surface tension.[16a] Thus, the exact mechanism that controls the LC pretilt angle on rubbed surface has not been unambiguously elucidated. Moreover, there are very few reports about the detailed research on the relationship between the pretilt angle and the conformation of alignment film.

The objectives of this research were to synthesize the organosoluble PIs having high pretilt angles and to investigate the effect of the conformation of the alignment film on controlling the pretilt angle. We focused on a specifically designed new aromatic PI containing *t*-butyl and trifluoromethyl pendent groups as an alignment layer having a high pretilt angle. The physical properties such as the thermal stability, chemical

* Corresponding author. Tel: +886-27376646. Fax: +886-27376644. E-mail: ytchern@mail.ntust.edu.tw.

10.1021/ma8022475 CCC: $40.75
Published on Web 12/16/2008

resistance, dielectric constant, and pretilt angle were investigated. The focus has especially been on the effect of the configuration of the PI alignment layer on the pretilt angle.

Experimental Section

Materials. Pyromellitic dianhydride (PMDA), 4,4′-oxidiphthalic anhydride (ODPA), 3,3′,4,4′-benzophenonetetracarboxylic dianhydride (BTDA), 4,4′-hexafluoroisopropylidene diphthalic anhydride (6FDA), 3,3′,4,4′-biphenyltetracarboxylic anhydride (BPDA), 3,3′,4,4′-diphenylsulfonetetracarboxylic dianhydride (SDA), and naphthalene-1,4,5,8-tetracarboxylic dianhydride (NTDA) were sublimated prior to use. *m*-Cresol was purified by distillation under reduced pressure over calcium hydride and was stored over 4 Å molecular sieves. Liquid crystals ZLI-2293 and 5CB were purchased from E. Merck Industries and were used as received. ZLI-2293 is a mixture of several compounds that contain various long alkyl chains and aromatic mesogens. It is in a nematic state at room temperature, and its isotropic transition temperature is 85 °C.

Instrumentation. A Bio-Rad FTS-40 FTIR spectrophotometer was used to record IR spectra (KBr pellets). In a typical experiment, an average of 20 scans per sample was made. Mass spectra were obtained by the use of a JEOL JMS-D300 mass spectrometer. ^{1}H and ^{13}C NMR spectra were recorded on Bruker AV 500 Fourier transform nuclear magnetic resonance spectrometers using tetramethylsilane (TMS) as the internal standard. A Perkin Elmer 240C elemental analyzer was used for elemental analysis. The X-ray crystallographic data were collected on a CAD-4 diffractometer. The analyses were carried out on a DEC station 3500 computer using NRCC SDP software. The melting points were obtained by a standard capillary melting point apparatus. Inherent viscosities of all polymers were determined at 0.5 g/dL using an Ubbelohde viscometer. Gel permeation chromatography (GPC) on soluble polymers was performed on an Applied Biosystem at 70 °C with two PLgel 5 μm mixed-C columns in the NMP/LiBr (0.06 mol/L) solvent system. The flow rate was 0.5 mL/min, detection was by UV, and calibration was based on polystyrene standards. Qualitative solubility was determined using 0.1 g of polymer in 2.0 mL of solvent. A TA Instruments DSC 2010 differential scanning calorimeter (DSC) and a PerkinElmer Diamond SII thermogravimetric (TG) analyzer were employed in the study of the glass-transition and thermal decomposition temperature of all of the polymers. The DSC was operated under a nitrogen stream at a flow rate of 30 cm^3/min and a heating rate of 20 °C/min. The TG analysis was determined under a nitrogen flow of 50 cm^3/min. Dynamic mechanical analysis (DMA) was performed on a TA Instruments DMA 2980 thermal analyzer system. A sample of 10 mm in length, 2 mm in width, and ~0.06 mm in thickness was used. The dynamic tensile mode was measured at 1 Hz frequency.

Tensile properties were determined from stress−strain curves with a Toyo Baldwin Instron UTM-III-500 apparatus with a load cell of 10 kg at a drawing speed of 5 cm/min. Measurements were performed at 28 °C with film specimens (about 0.1 mm thick, 1.0 cm wide, and 5.0 cm long), and an average of at least five individual determinations was used. Moisture absorption measurements were made with an ultramicrobalance of Sartorius model S3D-P on thin films (~40 μm). Measurements were operated by immersing films of these polyimides in distilled water at 25 °C for 100 h. Dielectric constants were measured by the sputter-coated sensor using a dielectric analyzer (TA Instruments DEA 2970) on thin films. Gold electrodes were vacuum-deposited on both surfaces of dried films, followed by being measured at 25 °C in a sealed chamber at 0% relative humidity. Contact angles of a deionized water and methylene iodide on the surface of the polyimide films were measured by a Ramé-Hart telescopic goniometer and Gilmont syringe with a 25 gauge flat-tipped needle. A Young's harmonic mean equation was applied to predict the surface tensions from the contact angles. XPS spectra were taken on a Thermo VG Scientific Theta Probe system. The electron takeoff angle is 37° from the sample surface. The surface morphology of the PI films was measured using an atomic force microscope (AFM, Digital Instruments, Nanoscope III). The AFM observation was performed under a tapping mode using a Si cantilever with a force constant of 28−48 N/m. A typical scan rate was ~0.5 Hz with 512 samples

Preparation of Alignment Layer and Cell. The synthesized soluble PIs were dissolved in a solvent including *N*-methyl-2-pyrrolidinone (NMP) and 2-ethoxyethanol (5:1) to form 6 wt % solutions. The glass substrates were cut into 2.5 × 3.0 cm^2 pieces. The PI solutions were spin-coated onto indium tin oxide (ITO) glass substrates at 2500 rpm, and the casts were baked at 90 °C for 10 min and at 200 °C for 2 h. The thickness of the PI layer was measured by an α-stepper to be in the 50−110 nm range. The PI-coated substrate was buffed two times (single direction) by a rubbing machine (Sigma Koki RM-50) with a 48 mm diameter roller covered with a cotton velvet cloth. The fiber length was 2 mm. The rubbing conditions were as follows: roller speed = 200 rpm, speed of substrate stage = 12 mm/s, and pile impression = 0.3 mm. Paired pieces from the same glass substrate were assembled together in the antiparallel rubbing direction by using 50-mm-thick spacers. A nematic LC, ZLI-2293, was injected into the cell gap, followed by sealing of the injection hole with an epoxy glue. The prepared LC cells were examined to be homogeneous through the whole cell by optical microscopy. The pretilt angles of the LCs on PI films were determined using a crystal rotation measurement carried out using an Autronic TBA 107 instrument.

2,6-Di-*tert*-butyl-4-(4-nitrophenyl)phenol (1). A 150 mL round-bottomed flask was charged with 2,6-di-*tert*-butylphenol (9.00 g, 43.6 mmol), potassium carbonate (6.60 g, 47.8 mmol), chloro-4-nitrobenzene (7.53 g, 47.8 mmol), and dry methyl sulfoxide (65.0 mL). The reaction mixture was heated to 105 °C for 22 h with stirring under N_2. Then, the reaction mixture was allowed to cool to room temperature and was poured in distilled water. The aqueous solution was acidified to pH 2 to 3, and yellow precipitate was collected by filtration. The yellow precipitate was washed with water and dried. The product was recrystallized from ethanol to afford 10.48 g (73.5%) of yellow crystals. mp 159−161 °C (lit.[17] mp 155−156 °C). IR (KBr): 1350, 1535, 2970, 3060, 3600 cm^{-1}. ^{1}H NMR ($CDCl_3$, δ): 1.43 (s, 18H, CH_3), 5.43 (s, 1H, OH), 7.43 (s, 2H, H-1), 7.83 (d, J = 8.25 Hz, 2H, H-2), 8.22 (d, J = 8.30 Hz, 2H, H-3). ^{13}C NMR ($CDCl_3$, δ): 30.89 (CH_3), 35.35 ($-C(CH_3)_3$), 124.48 (C-1), 124.68 (C-3), 127.90 (C-2), 129.90 (C-6), 140.35 (C-5), 146.43 (C-7), 148.75 (C-8), 155.99 (C-4). Anal. Calcd for $C_{20}H_{25}NO_3$: C, 73.40; H, 7.64; N, 4.28. Found: C, 73.25; H, 7.58; N, 4.25. Crystal data: $C_{20}H_{25}NO_3$; colorless crystal; 0.25 × 0.20 × 0.10 mm; monoclinic with a = 11.3820 (2) Å, b = 10.2860 (2) Å, c = 15.4040 (3) Å, α = 90°, β = 93.5380 (10)°, γ = 90° with D_c = 1.208 mg/m^3 for Z = 4, V = 1799.99 (6) Å^3, T = 295 K, λ = 0.71073 Å, F(000) = 704; Final R indices: R1 = 0.0560, wR2 = 0.1465.

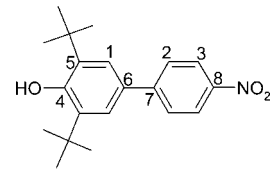

2,6-Di-*tert*-butyl-4-(4-nitrophenyl)-1-(4-nitro-2-trifluoromethylphenoxy)benzene (3). A mixture of 10.00 g (30.58 mmol) of **1**, 7.00 g (33.3 mmol) of 2-fluoro-5-nitrobenzotrifluoride, 4.70 g (34.0 mmol) of potassium carbonate, and 50.0 mL of dry *N*,*N*-dimethylformamide (DMF) was refluxed for 16 h under nitrogen. The reaction mixture was allowed to cool to room temperature, and the mixture was then poured in distilled water. The precipitate was collected by filtration and recrystallized from acetonitrile to afford 12.62 g (80.0%) of pale-yellow crystals. mp 220−223 °C. IR (KBr): 1356, 1532, 2960, and 3052 cm^{-1}. ^{1}H NMR ($CDCl_3$, δ): 1.27 (s, 18H, CH_3), 6.31 (d, J = 9.00 Hz, 1H, H-3), 7.64 (s, 2H, H-4), 7.76 (d, J = 10.06 Hz, 2H, H-5), 8.17 (d, J = 9.01 Hz, 1H, H-2), 8.32 (d, J = 10.04 Hz, 2H, H-6), 8.60 (s, 1H, H-1). ^{13}C NMR ($CDCl_3$, δ): 31.32 (CH_3), 35.92 (C-16), 116.14 (C-3), 117.65−118.40 (q, C-9), 119.01, 121.16, 123.32, 125.49 (q, CF_3), 124.16 (C-6),

124.31 (C-1), 126.44 (C-4), 127.90 (C-5), 128.47 (C-2), 136.52 (C-13), 141.09 (C-7), 144.38 (C-12), 147.15 (C-14), 147.23 (C-15), 151.31 (C-11). Anal. Calcd for $C_{27}H_{27}F_3N_2O_5$: C, 62.79; H, 5.23; N, 5.42. Found: C, 62.56; H, 5.28; N, 5.38.

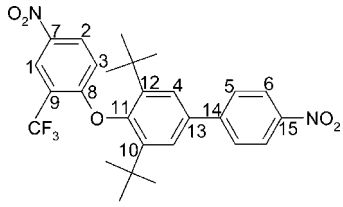

2,6-Di-*tert*-butyl-1-(4-nitrophenoxy)-4-(4-nitrophenyl)benzene (2). Compound **2** was synthesized from compound **1** (12.00 g, 36.7 mmol) and fluoro-4-nitrobenzene (5.70 g, 40.4 mmol) using the same procedure as that used for compound **3**. The product was recrystallized from acetonitrile to afford 9.02 g (54.9%) of pale-yellow crystals. mp 176−178 °C. IR (KBr): 1365, 1545, 2970, 3055 cm^{-1}. ^1H NMR ($CDCl_3$, δ): 1.30 (s, 18H, CH_3), 6.20 (d, $J = 9.50$ Hz, 1H, H-3), 7.25 (d, $J = 9.50$ Hz, 1H, H-2), 7.64 (s, 2H, H-5), 7.77 (d, $J = 7.00$ Hz, 2H, H-6), 8.05 (d, $J = 9.46$ Hz, 1H, H-4), 8.32 (m, 3H, $H = 1, 7$). ^{13}C NMR ($CDCl_3$, δ): 31.92 (CH_3), 36.20 (C-15), 114.58 (C-3), 117.63 (C-2), 124.39 (C-7), 125.91 (C-4), 126.55 (C-1), 126.63 (C-5), 128.13 (C-6), 136.19 (C-12), 142.29 (C-8), 144.74 (C-11), 147.33 (C-13), 147.81 (C-14), 152.06 (C-10), 166.16 (C-9). Anal. Calcd for $C_{26}H_{28}N_2O_5$: C, 69.60; H, 6.25; N, 6.25. Found: C, 69.54; H, 6.21; N, 6.22.

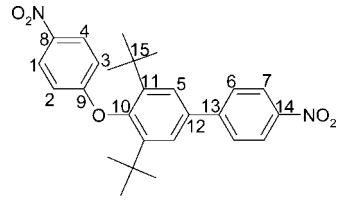

4-(4-Aminophenyl)-1-(4-amino-2-trifluoromethylphenoxy)-2,6-di-*tert*-butyl-benzene (5). A 150 mL, three-necked round-bottomed flask was charged with **3** (6.28g, 12.2 mmol), 44.0 mL of hydrazine monohydrate, 32.0 mL of ethanol, and 0.320 g of 10% palladium on carbon (Pd-C). The reaction mixture was heated to reflux for 4 days. The mixture was then filtered to remove the Pd-C, and the filtrate was poured in distilled water. The precipitate was collected by filtration, and the crude solid was recrystallized from hexane to yield 4.72 g (85.0%) of white crystals. mp 120−122 °C. IR (KBr): 1501, 1605, 2970, 3053, 3210, 3346, and 3445 cm^{-1}. ^1H NMR (DMSO-d_6, δ): 1.21 (s, 18H, CH_3), 5.02 (s, 2H, NH_2), 5.20 (s, 2H, NH_2), 5.79 (d, $J = 9.00$ Hz, 1H, H-3), 6.57 (d, $J = 9.02$ Hz, 1H, H-2), 6.65 (d, $J = 8.00$ Hz, 2H, H-6), 6.90 (s, 1H, H-1), 7.35 (d, $J = 8.04$ Hz, 2H, H-5), 7.45 (s, 2H, H-4). ^{13}C NMR (DMSO-d_6, δ): 31.24 (CH_3), 35.39 (C-10), 111.67 (C-1), 114.32 (C-6), 114.99−115.71 (q, C-9), 115.81 (C-3), 118.50 (C-2), 120.77, 122.95, 125.11, 127.29 (q, CF_3), 123.90 (C-4), 127.31 (C-5), 127.78 (C-14), 137.10 (C-13), 142.51 (C-7), 143.48 (C-12), 148.22 (C-8), 149.38 (C-15), 149.89 (C-11). Crystal data: $C_{27}H_{31}F_3N_2O$; colorless crystal; 0.25 × 0.20 × 0.10 mm; monoclinic with $a = 13.85600$ (10) Å, $b = 22.9810$ (3) Å, $c = 8.1000$ (2) Å, $\alpha = 90°$, $\beta = 102.6980$ (10)°, $\gamma = 90°$ with $D_c = 1.205$ mg/m^3 for $Z = 4$, $V = 2516.16$ (7) Å^3, $T = 295$ K, $\lambda = 0.71073$ Å, $F(000) = 968$; Final R indices: R1 = 0.0646, WR2 = 0.1820. Anal. Calcd for $C_{27}H_{31}F_3N_2O$: C, 71.05; H, 6.79; N, 6.14. Found: C, 70.83; H, 6.82; N, 6.11.

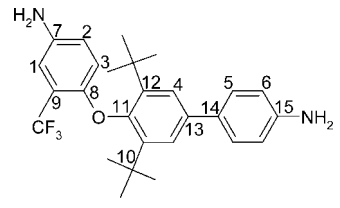

1-(4-Aminophenoxy)-4-(4-aminophenyl)-2,6-di-*tert*-butyl-benzene (4). Compound **4** was synthesized from compound **2** (5.50 g, 12.27 mmol) and hydrazine monohydrate (25.0 mL) using the same procedure as that used for compound 4. The product was recrystallized from toluene to afford 3.95 g (83.0%) of white crystals. mp 208−210 °C. IR (KBr): 1548, 1601, 2975, 3062, 3220, 3342, 3451 cm^{-1}. ^1H NMR (DMSO-d_6, δ): 1.25 (s, 18H, CH_3), 4.58 (s, 2H, NH_2), 5.16 (s, 2H, NH_2), 5.69 (brs, 1H, H-3), 6.34 (brs, 1H, H-4), 6.60 (brs, 1H, H-1), 6.67 (d, $J = 8.50$ Hz, 2H, H-7), 6.82 (brs, 1H, H-2), 7.34 (d, $J = 8.50$ Hz, 2H, H-6), 7.44 (s, 2H, H-5). ^{13}C NMR (DMSO-d_6, δ): 32.25 (CH_3), 36.09 (C-10), 114.99 (C-3, 4, 7), 116.25 (C-1), 117.20 (C-2), 124.50 (C-5), 127.91 (C-6), 128.83 (C-13), 137.14 (C-12), 143.02 (C-8), 144.16 (C-11), 148.69 (C-9), 151.07 (C-14), 153.08 (C-10). Anal. Calcd for $C_{26}H_{32}N_2O$: C, 80.41;

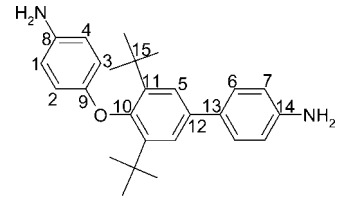

H, 8.24; N, 7.21. Found: C, 80.36; H, 8.20; N, 7.18. Crystal data: $C_{26}H_{32}N_2O$; colorless crystal; 0.25 × 0.20 × 0.20 mm; monoclinic with $a = 15.188$ (2) Å, $b = 19.084$ (3) Å, $c = 16.149$ (3) Å, $\alpha = 90°$, $\beta = 95.5430$ (10)°, $\gamma = 90°$ with $D_c = 1.108$ mg/m^3 for $Z = 8$, $V = 4658.87$ (13) Å^3, $T = 295$ K, $\lambda = 0.71073$ Å, $F(000) = 1680$; Final R indices: R1 = 0.0691, WR2 = 0.1874.

Representative Procedure for the Preparation of Polyimides (7 and 8). Polymerization was carried out in a one-step chemical imidization. The diamine **5** (1.012 g, 2.22 mmol), PMDA (0.485 g, 2.22 mmol), and *m*-cresol (10.0 mL) were added to a three-necked flask equipped with a stirrer, a nitrogen inlet, and a distillation head. Isoquinoline (6 drops) was added to the flask. After the mixture was stirred at room temperature for 3 h and heated to 80 °C for 2 h, it was heated to 200−210 °C for 14 h. Water was continuously distilled from the reaction mixture. The solution was poured in methanol (500 mL). The polymer that precipitated was collected, filtered, washed with ethanol and water, and dried under reduced pressure at 200 °C for 8 h. The yield of polyimide was 95%. The inherent viscosity of **8a** was 0.80 dL/g, as measured at a concentration of 0.5 g/dL in NMP at 30 °C. IR (KBr): 2970,1784, 1720, 1381 cm^{-1}. ^1H NMR (DMSO-d_6, δ): 1.26 (18H, CH_3), 6.38 (1H, H-3), 7.64−7.76 (6H, H-1, 2, 4, 5), 7.98 (2H, H-6), 8.38 (2H, H-7).

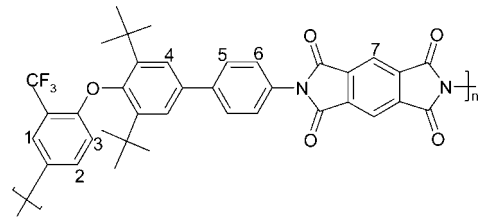

2,6-Di-*tert*-butyl-1-(4-phthalimidophenoxy)-4-(4-phthalimidophenyl)benzene (6). The diamine **4** (0.772 g, 1.99 mmol), phthalic anhydride (0.591 g, 3.98 mmol), and *m*-cresol (10 mL) were added to a three-necked flask equipped with a stirrer and a nitrogen inlet. Isoquinoline (6 drops) was added to the flask. After the mixture was stirred at room temperature for 3 h, it was heated to 200−210 °C for 14 h. The solution was poured in a hot water (500 mL). The product that precipitated was collected, filtered, washed with ethanol and water, and dried under reduced pressure at 200 °C for 8 h. The yield of **6** was 92%. IR (KBr): 2970, 1784, 1720, and 1381 cm^{-1}. Crystal data: $C_{42}H_{36}N_2O_5$; colorless crystal; 0.80 × 0.20 × 0.05 mm; triclinic with $a = 6.1214$ (1) Å, $b = 13.9147$ (2) Å, $c = 20.1861$ (4) Å, $\alpha = 99.6105$ (6)°, $\beta = 97.7764$

Scheme 1

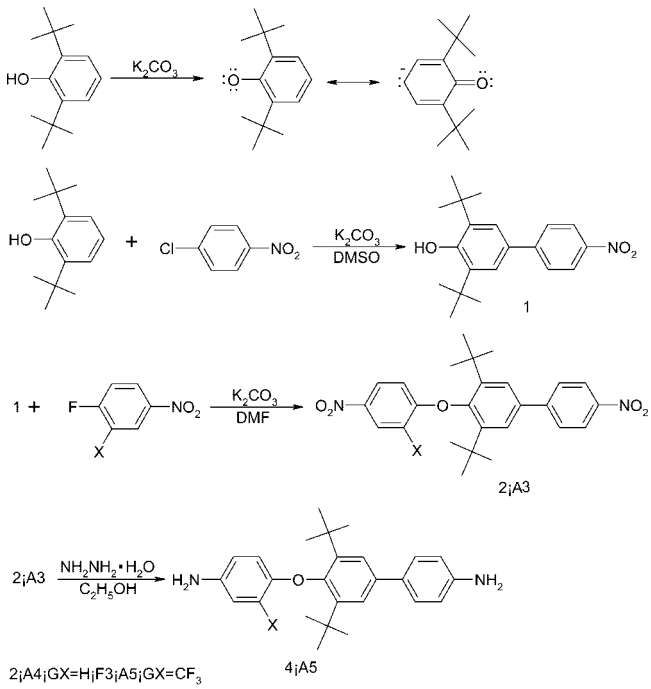

(8)°, γ = 90.2326 (9)° with D_c = 1.283 mg/m^3 for Z = 2, V = 1679.05 (5) Å^3, T = 295 K, λ = 0.71073 Å, μ= 0.084 mm^{-1}, F(000) = 684; final R indices: R1 = 0.1003, WR2 = 0.2725.

Results and Discussion

Monomer Synthesis. Three steps were employed in synthesizing the new diamines (**4** and **5**) from 2,6-di-*tert*-butylphenol, as shown in Scheme 1. The 2,6-di-*tert*-butylphenoxide ion shows two resonance structures (Scheme 1). Given the steric hindrance of oxygen, the nucleophilic character of the para carbon is dominant, and an aromatic nucleophilic substitution (S_NAr) reaction occurs at that position to produce compound **1**. The yield of **1** was high at 73.5 %. The high yield suggests that the nucleophilic character of the para carbon is dominant (Scheme 1). An S_NAr reaction of **1** with 1-fluoro-4-nitrobenzene and 2-chloro-5-nitrobenzotrifluoride in DMF in the presence of potassium carbonate as an acid acceptor generated the dinitro compounds **2** and **3**, respectively, which were then hydrogenated to generate the new diamines **4** and **5**, respectively. Elemental analysis, IR, and NMR spectroscopic techniques were used to identify structures of the intermediate compounds (**1**, **2**, and **3**) and the target diamine monomers (**4** and **5**). The ^{1}H NMR spectra of the monomers (**2** and **4**) are shown in Figure 1. Interestingly, in the ^{1}H NMR spectrum of compound **2**, H-2 and H-3 are not magnetically equivalent, and H-1 and H-4 are not magnetically equivalent. This is because the steric hindrance of the bulky *tert*-butyl groups prevents the benzene ring of the 4-aminophenoxy moiety from rotating freely. Moreover, H-3 appeared farthest upfield at 6.20 ppm (Figure 1a) because of the ring current effect caused by neighboring benzene. Compound **4** showed the same behavior, and H-3 appeared farthest upfield at 5.69 ppm (Figure 1b). Interestingly, H-1 to H-4 produced individual broad singlet signals (Figure 1b). In the ^{13}C NMR spectrum of compound **3**, C-9 and CF_3 showed clear quartet absorptions at 117.65 to 118.40 and 119.01 to 125.49 ppm, respectively, because of the coupling of the carbons to fluorine atoms (Experimental Section). The diamine **5** also exhibited the same behavior with quartet absorption in its ^{13}C NMR spectrum. The signals that appeared at 4.58 and 5.16 ppm were peculiar to the amino groups (Figure 1b). Elemental analysis results, the NMR spectra, and the IR spectra confirmed

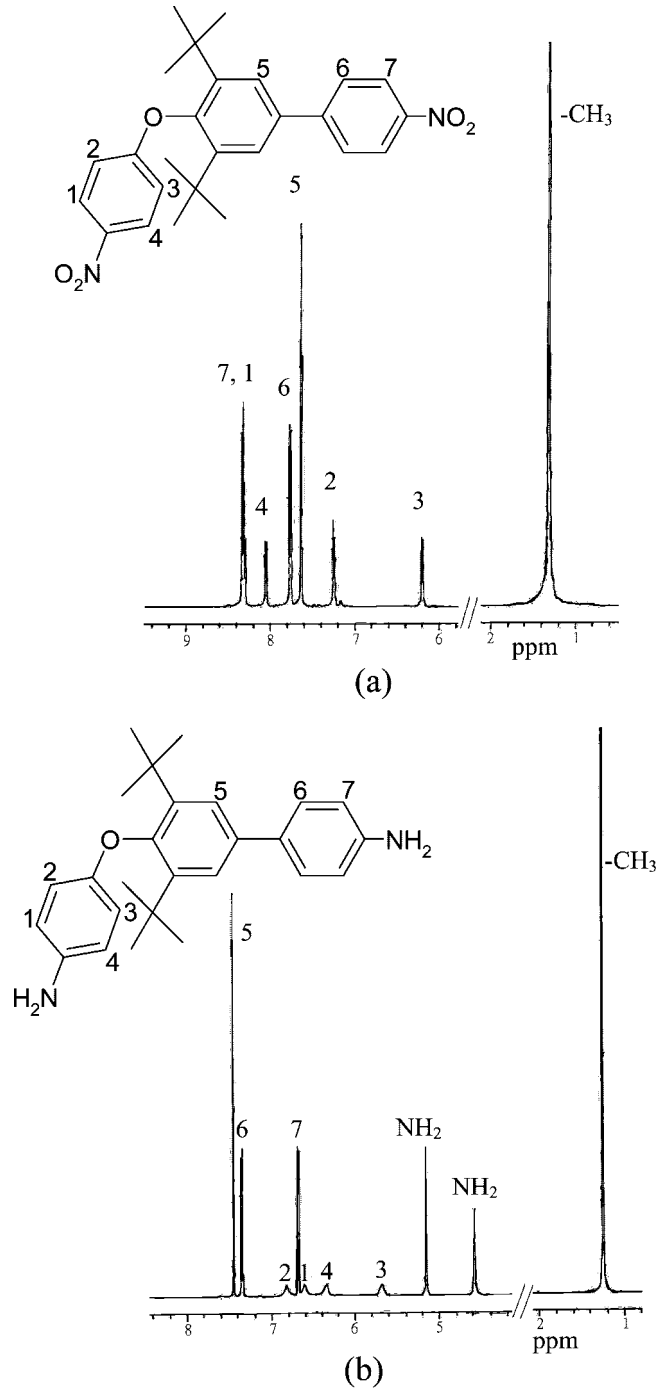

Figure 1. ^{1}H NMR (500 MHz) spectra of (a) **2** and (b) **4**.

the structures of all compounds reported herein. In addition, X-ray diffraction analysis also confirmed the structures of **4** and **5** (in Figure 2). X-ray crystal data for **4** and **5** were acquired from an individual single crystal, as obtained by slowly crystallizing from toluene and hexane solutions, respectively. In the X-ray structure of **4**, the dihedral angles between the central and outer rings are 85 and 37° for C(1)−C(2) and C(13)−C(14), respectively (in Figure 2a). In the X-ray structure of **5**, the dihedral angles between the central and outer rings are 84 and 25° for C(1)−C(2) and C(14)−C(15), respectively (in Figure 2b). The structures of **4** and **5** exhibited asymmetrical and bulky molecular characteristics.

Synthesis of Polyimides. The polyimides were prepared by the one-step method in *m*-cresol at 200−210 °C (Scheme 2). The formation of PIs was confirmed by IR and ^{1}H NMR

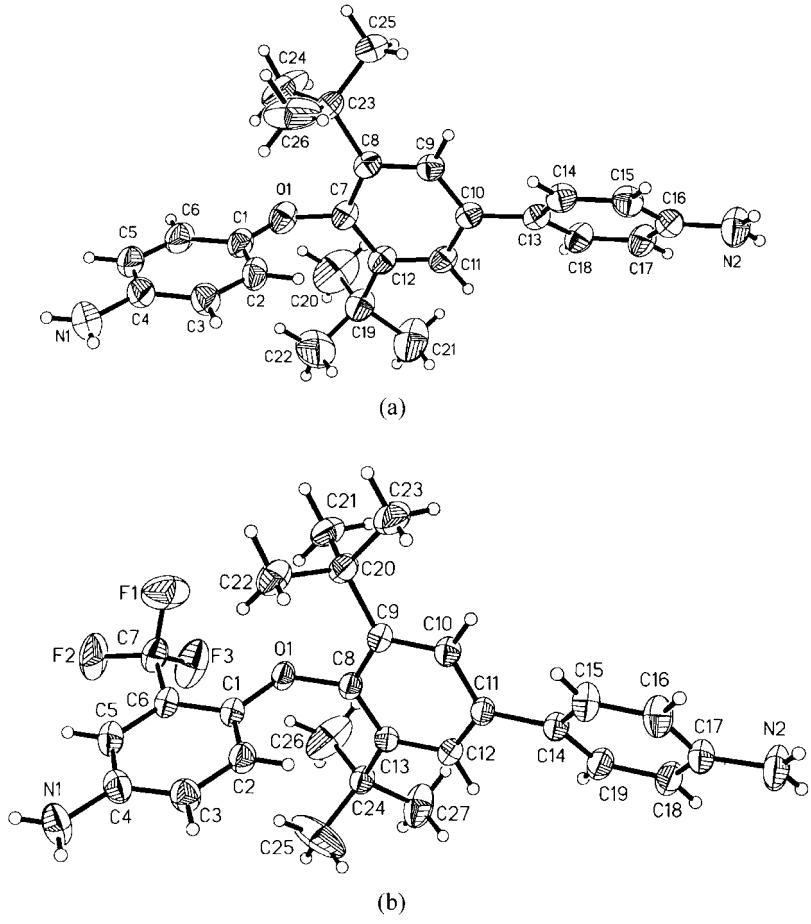

Figure 2. X-ray structures of (a) **4** and (b) **5**.

Scheme 2

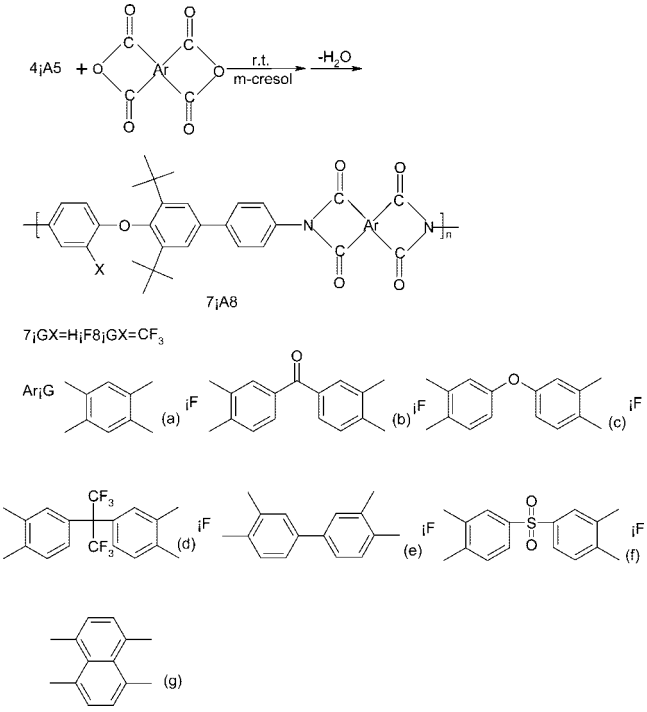

spectroscopy (see the Experimental Section). The inherent viscosities and GPC molecular weights of PIs are shown in Table 1. The **7** and **8** series soluble PIs had high inherent viscosities of 0.90 to 1.20 and 0.74 to 2.31 dL/g, respectively. Table 1 also indicates that the M_n values of PIs **7** and **8** are

Table 1. Inherent Viscosities and GPC Molecular Weights of Soluble Polyimides

polymer	η_{inh}[a]	$M_n \times 10^{-4}$[b]	M_w/M_n
7a	1.02	[c]	
7b	1.20	3.2	2.5
7c	0.97	3.0	2.0
7d	0.90	3.4	2.4
7e	1.00	3.1	2.2
7f	0.97		
8a	0.80	3.1	2.3
8b	1.38	5.2	2.4
8c	0.84	3.2	2.2
8d	0.81	4.1	2.2
8e	0.74	3.0	2.1
8f	1.22	5.5	2.3
8g	2.31	10.5	2.2

[a] Measured in NMP on 0.5 g/dL at 30 °C. [b] By GPC (relative to polystyrene). [c] Could not be measured.

30 000−34 000 and 30 000−105 00, respectively. The inherent viscosity of the rigid-rod PI **8g** based on NTDA was higher than that of the PIs prepared from the other anhydrides. The flexible and tough PI films **7** and **8** were obtained by casting from their NMP solution onto a glass plate and drying at 200 °C for 5 h under reduced pressure.

Characterization of Polymers. The solubilities of these polyimides were tested in various solvents. Table 2 summarizes those results. The **7** and **8** series PIs show very good solubility in the tested solvents. It is well known that aromatic PIs generally show rather poor solubility in organic solvents, especially for those derived from rigid dianhydrides such as PMDA and NTDA. Although the **7** PIs derived from nonfluorinated diamine 4 had good solubility, the **7b**, **7c**, and **7e** PIs were soluble in NMP, DMAc, *m*-cresol, chloroform, THF, and

Table 2. Solubility of Polyimides[a]

polymer	NMP	DMAc	*m*-cresol	$CHCl_3$	THF	cyclohexanone
7a	++	+	++	−	−	−
7b	++	++	++	+−	++	++
7c	++	++	++	++	++	++
7d	++	++	++	++	++	++
7e	++	++	++	++	++	+
7f	++	++	++	−	−	+
8a	++	++	++	−	++	++
8b	++	++	++	++	++	++
8c	++	++	++	++	++	++
8d	++	++	++	++	++	++
8e	++	++	++	++	++	++
8f	++	++	++	++	++	++
8g	++	++	+	++	++	+−

[a] Solubility: ++, soluble at room temperatures; +, soluble on heating at 60 °C; +−, partial soluble in heating at 60 °C, −, unsoluble. Abbreviations: NMP, *N*-methyl-2-pyrrolidinone; DMAc, *N*,*N*-dimethylacetamide; THF, tetrahydrofuran.

Table 3. Physical Properties of Polyimide Films

polymer	tensile strength (MPa)	elongation at break (%)	% H_2O absorption[a]	dielectric constant (dry, 1 KHz)
7a	65	10.2	1.48	2.95
7b	82	5.9	1.53	3.10
7c	88	16.0	1.49	2.98
7d	83	21.4	0.97	2.82
7e	100	18.7	1.15	3.05
7f	88	4.3	1.74	3.11
8a	63	11.8	1.05	2.93
8b	74	35.3	0.97	3.02
8c	79	23.9	0.73	2.85
8d	71	53.2	0.65	2.75
8e	67	25.3	1.02	2.95
8f	82	20.8	1.42	3.01
8g	69	47.6	0.96	2.94
ref 1[b]	135	17.6	2.56	3.30

[a] Moisture absorption of polyimide films was measured by immersing these polyimide films in distilled water at 25 °C for 100 h. [b] Polyimide was synthesized from 4,4′-oxydianiline (ODA) and pyromellitic dianhydride (PMDA) in our laboratory. The inherent viscosity of its poly(amic acid) precursor was 1.25 dL/g.

cyclohexanone. It is surprising that PI **7a**, which was prepared from the rigid PMDA, was soluble in NMP, DMAc, and *m*-cresol. The increased solubility of the **7** series is ascribed to the reduced intermolecular force between the polymer chains due to the introduction of asymmetric di-*tert*-butyl groups. Because of the introduction of trifluoromethyl groups in **8** series PIs, **8** series had better solubility than **7** series. For example, PI **8a** derived from the rigid PMDA was soluble in THF and cyclohexanone at room temperature, whereas the polymer **7a** was not soluble in THF and cyclohexanone, even upon heating. Even PI **8g** derived from the rigid NTDA was soluble in NMP, DMAc, *m*-cresol, chloroform, and THF. The increased solubility of the **8** series is ascribed to the fact that the introduction of asymmetric trifluoromethyl groups in the polymeric side group leads to a decrease in intermolecular force between the polymer chains. One of the most important applications of PI is its use in LC alignment layers for LC flat-panel display devices. Conventional PI materials that require curing temperatures above 250 °C are not suitable for use in the fabrication of full-color LCDs that use color filters containing dyes or organic pigments that are not stable above 200 °C. It is necessary to use organic soluble PI alignment films that can be cured below 200 °C.

Table 3 summarizes the dielectric constants, moisture absorptions, and mechanical properties of the films. The mechanical properties were determined by an instron machine. The mechanical properties of the **7** and **8** series PIs, in general, are satisfactory. All **7** and **8** series PIs exhibited moderate tensile strength of 65−100 and 63−82 MPa, respectively, and they also gave fairly high values of elongation at break. The moderate tensile strengths of **7** and **8** series PIs were due to the decreased intermolecular force between the polymer chains. The **7** series PIs had slightly better tensile strengths than did the corresponding **8** series PIs. The low values of the tensile strength of the **8** series is attributed to the presence of asymmetric trifluoromethyl and *tert*-butyl groups in the bulky pendent groups, which result in a weakness intermolecular force between the polymer chains. It is surprising that **8** series PIs exhibited high elongation-at-break values. For example, elongation-at-break values of **8d** and **8g** were 53.2 and 47.6%, respectively. We measured moisture absorption of PI films by immersing these PI films in distilled water at 25 °C for 100 h. The moisture absorption of **7** and **8** series polymers is low, that is, <1.74%, because of the water proofing effect of the *tert*-butyl and trifluoromethyl groups. Because of the polar of the sulfone group, **7f** and **8f** had relatively high moisture absorption. The **7** and **8** series PIs containing the *tert*-butyl and trifluoromethyl groups in the main chain also exhibited low dielectric constants in the range of 2.75 to 3.11, which is significantly lower than that (3.3) of PI film prepared from PMDA and 4,4′-oxidianiline. The hexafluoroisopropylidene-containing PIs **7d** and **8d** had lower dielectric constants than the other **7** and **8** series PIs. The low values of the dielectric constants might be attributed to the presence of trifluoromethyl groups in the bulky pendent groups, which result in a weakness between the polymer chain and the polymer chain electronic interaction because of the low electronic polarizability of the fluorine atoms. In addition, such low dielectric constants are also due to the fact that the asymmetric *tert*-butyl group loosened the polymer chain packing, which subsequently lead to a reduction in the density.

Table 4. Thermal Properties of Polyimides

	T_g (°C)		T_d (°C)[c]		
polymer	DSC[a]	DMA[b]	in air	in N_2	char yield (%)[d]
7a	395	402	490	491	41
7b	337	358	495	494	41
7c	337	347	495	499	42
7d	346	364	490	496	40
7e	374	389	505	502	43
7f	344	365	462	454	33
8a	[e]	420	481	480	38
8b	358	366	482	480	36
8c	353	353	482	488	34
8d	356	369	475	486	33
8e	382	396	488	490	35
8f	363	368	450	453	30
8g		456	491	489	35

[a] Temperature at which the middle of change of the heat capacity occurred from the second DSC heating scan at a heating rate of 20 °C/min. [b] Temperature at which the peak maximum of tan δ occurred as recorded by DMA at a heating 5 °C/min. [c] Temperature at which 10% weight loss recorded by thermogravimetry at a heating rate of 10 °C/min. [d] Residual wt % at 800 °C in nitrogen. [e] No T_g was obtained.

The thermal stability of these polyimides was investigated by DSC, DMA, and TGA. The thermal properties of **7** and **8** series PIs are listed in Table 4. Dynamic thermogravimetry showed the relatively good thermal stability of **7** and **8** series PIs. The temperature at weight loss of 10% exceeds 450 °C. In DSC measurements, most of the **7** and **8** series PIs showed distinct baseline shifts on their DSC heating traces glass-transition temperatures (T_g), defined as the temperature at the midpoint of the baseline shift; all PIs had high T_g values (>337 °C). The T_g values of the **8** series were about 8−21 °C higher than those of the corresponding **7** series. The high T_g values for **8** series PIs could be attributed to the fact that the *tert*-butyl groups of the biphenyl moiety in the backbones are prohibited from free rotation by the steric hindrance of the trifluoromethyl groups, resulting in an increased chain stiffness. More detailed information can be obtained from the dynamical measurements

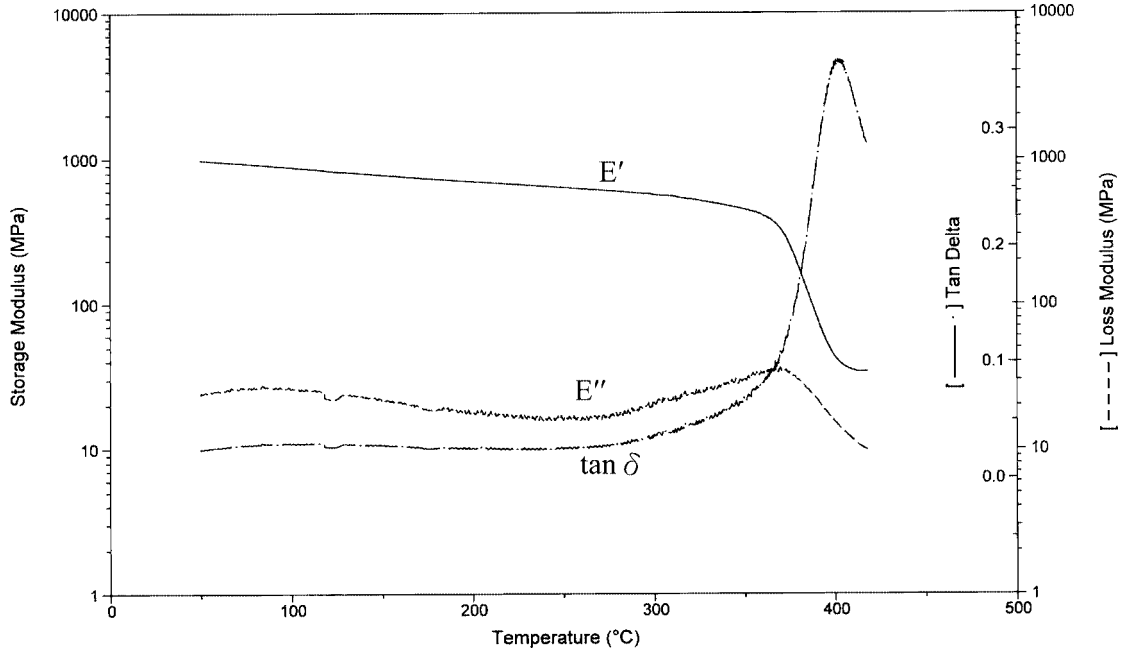

Figure 3. Dynamic mechanical analysis curves for **7a** at a heating rate of 5 °C/min.

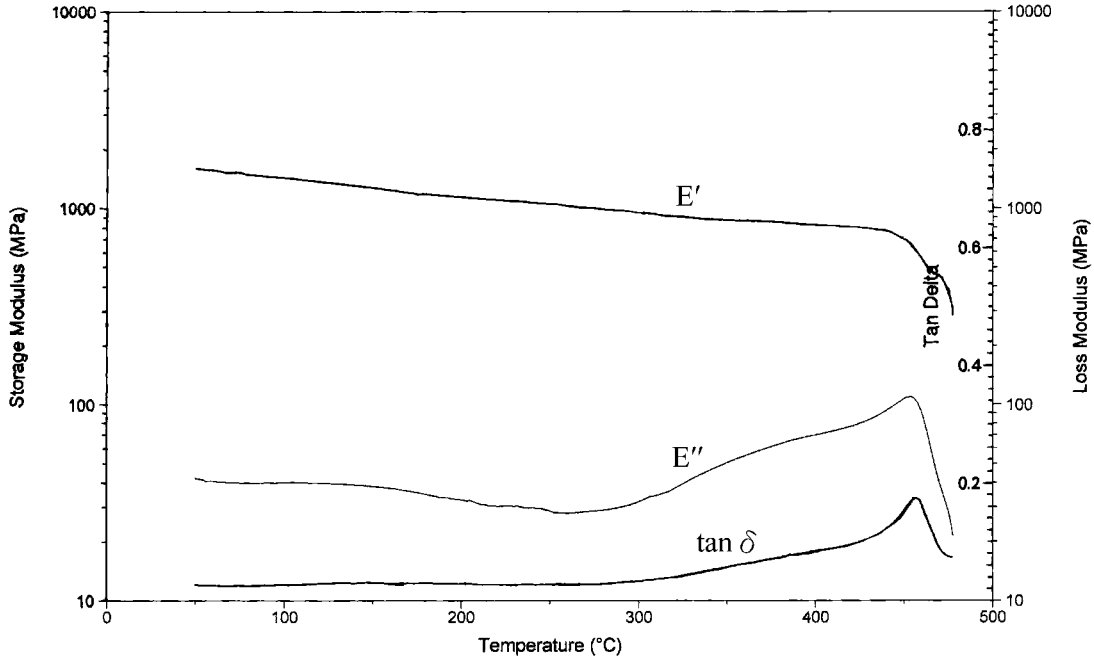

Figure 4. Dynamic mechanical analysis curves for **8g** at a heating rate of 5 °C/min.

of these polyimide films. Herein, the mechanical properties of these polyimide films (~60 μm in thickness) were studied between 0 and 500 °C. Figure 3 depicts mechanical relaxation spectra of PI **7a**. On the basis of tan δ and E' peaks, one relaxation was observed at 402 °C. The glass transition at ~402 °C is associated with an approximately 1 order of magnitude decrease in E'. Figure 4 illustrates the mechanical relaxation spectra of **8g**. On the basis of tan δ and E'' peaks, the glass transition was observed at 456 °C. The E' of **8g** was found to remain high (0.8 GPa) at 425 °C. It is noteworthy that the soluble PI **8g** has a very high T_g (456 °C). The high T_g materials are important for high-temperature applications. The mechanical relaxation spectra of the other PIs (**7** and **8** series) resemble those of **7a**. Table 4 also summarizes the glass-transition temperatures measured by DMA. These polyimides exhibited high T_g (>347 °C). The higher T_g values, that is, **7a**, **8a**, and **8g**, are attributed to the fact that the rotations of these bonds are hindered by the rigid structures within the dianhydride (PMDA and NTDA) moieties of the PIs, causing chain stiffness to increase.

Conformations of Compound 6. To elucidate the generation mechanism of the high pretilt angle in more detail, we investigated the conformations of PIs by using single-crystal analyses of small molecules. Bond lengths and bond angles vary only very slightly between closely related molecular systems, so reliable data of this type can be obtained from single-crystal analyses of small molecules related to the polymer in question. For example, Tashiro et al. reported that the planar conformation of the chain and the translational shifts between the neighboring chains are quite similar for the poly(*p*-phenylene benzobisoxazole) and model compounds.[18] Herein, single-crystal studies

of oligomers containing a repeat unit of the polymer itself can provide strong indications of the preferred values of torsion angles within and between monomer residues, though these values are naturally less constrained than are the bonding parameters. Single crystals of compound **6** that were suitable for X-ray analysis were grown by slow evaporation of solution in NMP. Figure 5 shows various views of the crystal structures and packing of compound **6**. Compound **6** adopts a much more generally extended conformation. This geometry is achieved by a combination of (i) a relationship between rings A and B that is closer to being orthogonal than planar (inter-ring torsion angle 86°, 120° bond angle at oxygen), (ii) a relationship between rings A and D that is near planar (inter-ring torsion angle 26°), (iii) a similar relationship between ring A and the imide unit E that is near planar (inter-ring torsion angle 14°), and (iv) an inter-ring torsion angle between the imide unit F and the ring B of 51°. The distance from the ring H centroid to O(1) is 13.22 Å, and the distance from the ring G centroid to O(1) is 8.94 Å (Figure 5). In addition, the distance from C(38) to C(41) is 7.20 Å. Figure 5b also shows that the oxygen of the pyromellitimide unit particularly interacts with a hydrogen of the adjacent benzene ring (O(4)···H−C(15A); O(4)···H−C(24B)) in the lattice as dashed lines.

The imide unit E and the ring A are almost coplanar for compound **6** (Figure 5). Note that the two planes on both sides of the ether linkage are nearly orthogonal (i.e., inter-ring torsion angle 86°, Figure 5). Clearly, the conformation of compound **6** created the two orthogonal planes (Figure 5b). Although the PI **7** films used in this study are amorphous, the local structure of a molecule (PI **7**) is thought to be similar to the crystalline structure of compound **6**. In general, the rigid PI films align spontaneously parallel to the film plane (in-plane orientation) upon thermal cure reaction. From these results, we speculated that the orthogonal planes on both sides of the ether linkage, in which the sequences of near in-plane orientation and out-of-plane orientation were arranged in an alternating fashion, were generated by the **7a** and **7g** PIs. A schematic drawing of the alternately flat-straight structures of **7a** is shown in Figure 6. The long edge of the plane measured ∼22.16 Å, as calculated from a single crystal data of compound **6** (Figure 6).

Polyimide Alignment Layers Having High Pretilt Angles. Some reports have pointed out that an alkyl side chain greatly elevates the pretilt angle.[4c,7,8b,9e,12,15] As widely reported, the long alkyl side chain with more than 10 carbon atoms is well known for its positive effect on the LC alignment and the achievement of a high pretilt angle.[15b] For example, Wang reported that the pretilt angle generated by a film of the polyimide prepared from C12 was only 6°.[12b] When the length of the side chain was increased to C14 and C16, the corresponding films generated pretilt angles of 90°. To achieve a high pretilt angle, Seo et al. also reported that the large pretilt angle for 5CB generated on rubbed PI surfaces is associated with CF_3 moieties attaching to the lateral benzene ring.[4d,e] However, the pretilt angle of 5CB is small on PI surfaces with CF_3 moieties attached to the polymer backbone.

Table 5 summarizes the pretilt angles of ZLI-2293 LC molecule on the PI coating surfaces. Surprisingly, **7a**, **8a**, and **8g** PIs had high pretilt angles of 87.9 to 88.7° after the rubbing process (Figures S1−S3 in the Supporting Information) and were independent of thermal annealing. These unusually high pretilt angles are quite different from those in earlier reports on the rigid PI alignment layers, where the pretilt angles were <10°.[4d,7,12] To the best of our knowledge, there have been no reports that such a high pretilt angle (>30°) was achieved using the fully rigid aromatic PIs without long side chains. This is the first study that achieved a high pretilt angle using the rigid PI. Even **8a** also had a high pretilt angle above 89° before the rubbing process (Figure S4 in the Supporting Information). The rubbed aromatic PI (PMDA−ODA, Table 5), which is chemically similar to the backbones of **7a** and **8a**, resulted in a low pretilt angle (1.27°). These results indicate that the pretilt angle of bulk LCs is unambiguously associated with the intrinsic PI chemical architectures. The *tert*-butyl side groups play a vital role in generating the high pretilt angles of bulk LCs. This unexpected finding is associated with the specific conformation in the film surface of PI. In addition, this study found that these alignment layers are stable in the presence of temperature changes. When the temperature increases from 30 to 70 °C, the pretilt angles of **7a**, **8a**, and **8g** were found to remain above 88°. The pretilt angles of **8a** and **8g** were found to remain above 88° after annealing at 65 °C for 72 h. Additionally, the pretilt angle of 5CB molecules on a rubbed **8a** film was 89°.

To understand the surface morphology of the rubbed PI films, we observed the surfaces of the PI films after rubbing using the AFM technique. Figure 7 shows a typical topographical image of a rubbed PI film. The rubbed **8a** and **8g** developed microgrooves that ran parallel to the rubbing direction, which resembles those reported for rubbed films of PIs.[7,9] The microgroove lines that were generated might be due to the shear-induced deformation of the polymer film surface induced by the contact of fibers during the rubbing process. The developed microgrooves of **8a** and **8g** were around 235 and 150 nm in size, respectively. The surface roughness values across the rubbing direction of the area marked in Figure 7 for the rubbed **8a** and **8g** films were 1.07 and 0.512 nm, respectively. Overall, the microgrooves developed along the rubbing direction are much larger in size than the LC molecules. Therefore, it is believed that the molecular chain reorientation has a greater influence on the LC aligning ability of the PI film surfaces than do the microgrooves.

To understand the microscopic surface structure at the rubbed PI alignment layer, we conducted the measurement of contact angles and the X-ray photoelectron surface analysis. Table 6 shows the contact angles of the water and the diiodomethane on the PI films, from which the surface energies were calculated by the harmonic-mean equation before and after the rubbing.[19] The surface energies of the tested **7a**, **8a**, and **8g** PIs ranged from 41.6 to 47.9 dyn/cm. The surface energies of the tested PIs did not significantly change by rubbing. The PI surface energies in previous studies were <40 dyn/cm, which tended to create high pretilt angles.[4b,16b] Although **7a**, **8a**, and **8g** PIs in this study had high surface energies, their alignment layers with high pretilt angles (>87.9°) were achieved by rubbing. From these results, it can be seen that the pretilt angles of the LC cell using **7** and **8** series PIs were affected by the geometric structure of the PI film surfaces, not the surface energy. The atomic composition of the alignment layer's outer layer was also determined before and after rubbing by XPS. However, the XPS atomic compositions remained unchanged by rubbing. The almost no difference between the atomic compositions of **7** and **8** series PIs by XPS might be attributed to the fact that the atomic composition of the class of **7** and **8** series PIs did not have a distinct change in the rubbing-induced deformation. However, the PI molecules oriented along the rubbing direction generated a new geometric surface structure. The geometric surface structure plays a very important role in controlling the LC pretilt angle.

Considering the PI film conformation results presented above, the conformations of **7a** were the alternative flat-straight structures. In general, rigid PI films align spontaneously parallel to the film plane (in-plane orientation) upon thermal cure reaction. The **7** and **8** series PIs belong to the analogue of the rigid PIs. PI **7a** exhibited the alternative flat-straight structure described above. Thus, we speculated that the conformation of

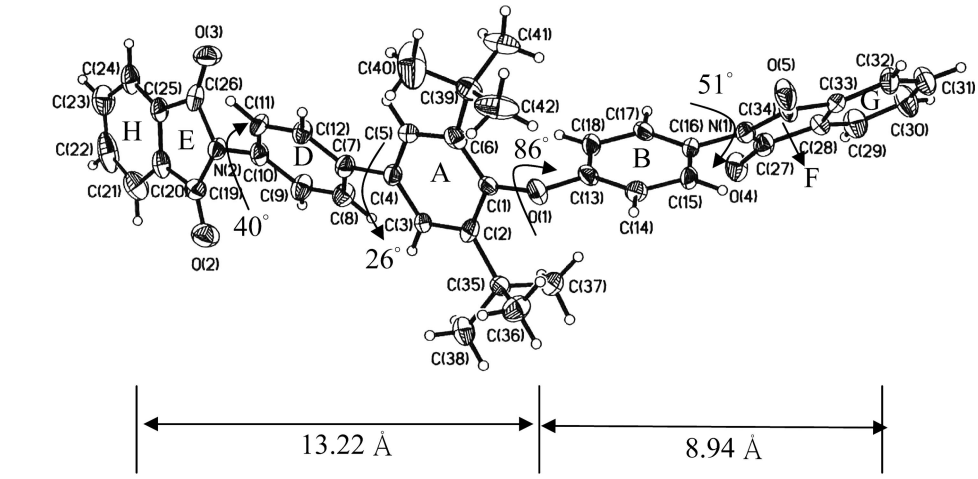

(a)

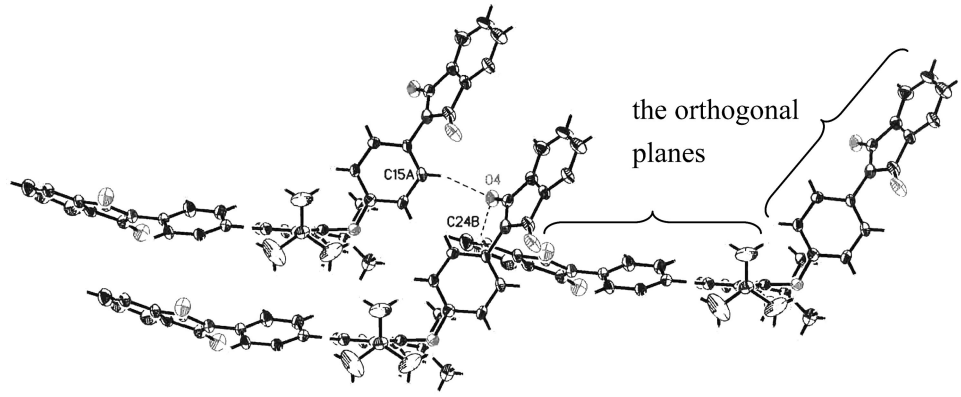

(b)

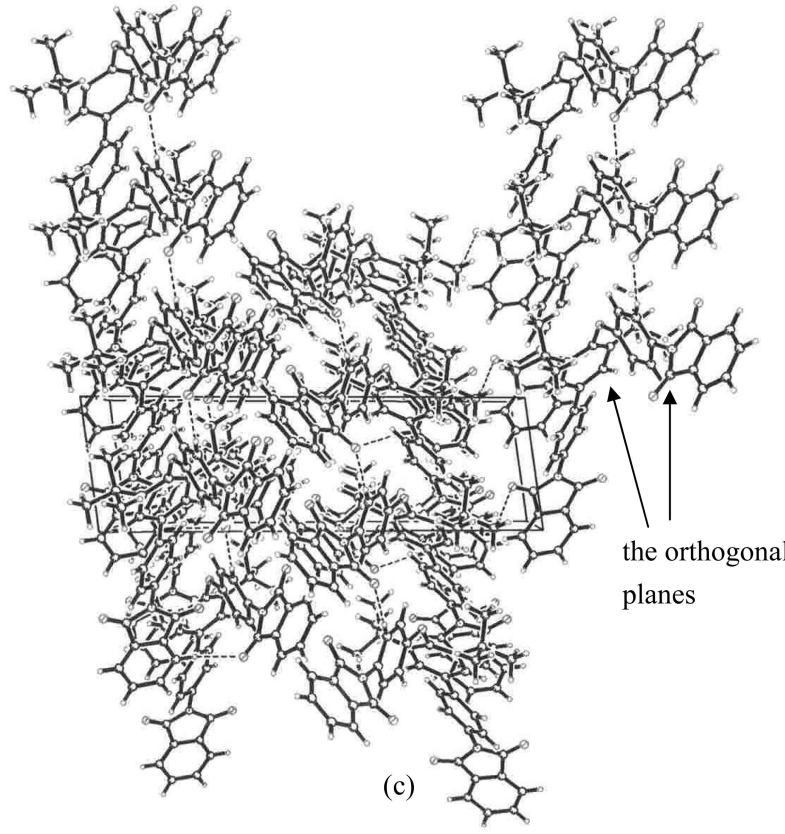

(c)

Figure 5. (a) ORTEP diagram, (b) one trimeric pair, and (c) crystal packing view along the *b* axis of compound **6**.

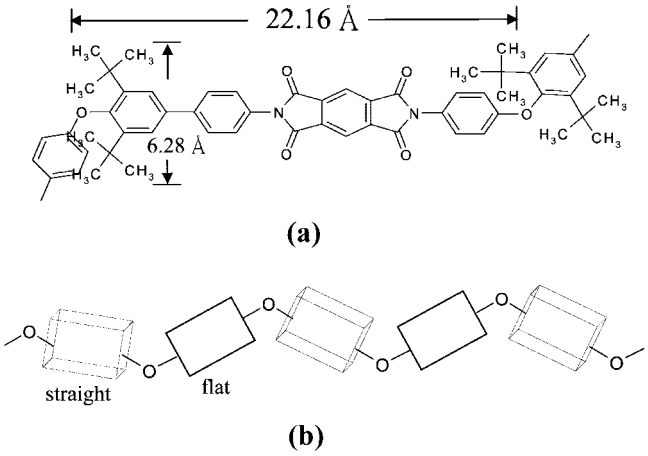

Figure 6. (a) Chemical structure of PI **7a** and (b) a schematic drawing of the geometric surface structure of PI **7a**.

Table 5. LC Pretilt Angle (θ_p) on Various Polyimides

alignment layer polymer	θ_p, deg unrubbed[a]	θ_p, deg rubbed[b]
7a	0.7	87.9(88.3)[c]
7b	0.5	0.6
7c	0.3	0.5
7d	0.8	1.2
7e	0.6	0.7
7f	0.5	1.3
7g	0.6	0.4
8a	89.5(89.4)	88.7(88.5)
8b	0.63	1.2
8c	0.92	1.3
8d	0.3	0.9
8e	0.8	0.5
8f	0.6	0.8
8g	0.2	88.3(88.2)
ref 1[d]		1.27

[a] The polymer was spin-coated and cured between 90 and 200 °C. [b] Rubbing conditions: roller speed, 200 rpm; speed of substrate stage = 12 mm/s; pile impression = 0.3 mm; and rubbed twice in the same direction. [c] Data in parentheses are pretilt angles on various LC cells after annealing at 50 °C for 10 min. [d] A poly(amic acid) precursor(η_{inh} = 1.25dL/g) was spin-coated and cured between 100 and 320 °C.

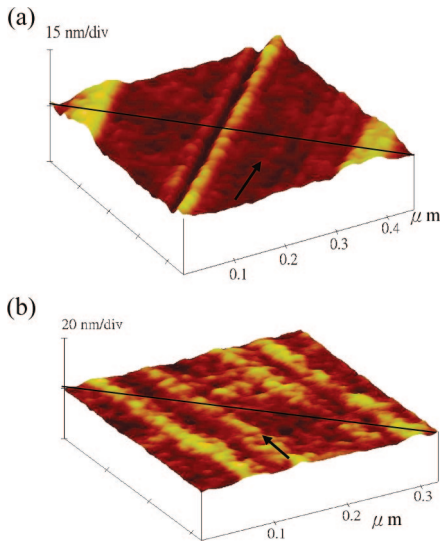

Figure 7. AFM images and surface profiles of polyimide films after rubbing: (a) **8a**; (b) **8g**. The arrow in each AFM image denotes the rubbing direction.

PI **7a** was the alternating sequences of near in-plane orientation and out-of-plane orientation. The homeotropical alignment

Table 6. Surface Energy of Polyimides before and after the Rubbing Process

polymer	condition	contact angle (deg) water	contact angle (deg) diiodomethane	surface energy (dyn/cm)
7a	unrub[a]	75.3	27.6	46.4
7a	rub[b]	82.3	23.3	46.8
8a	unrub	78.7	25.9	46.3
8a	rub	73.6	24.0	47.9
8g	unrub	87.0	36.0	41.6
8g	rub	82.3	35.0	42.4

[a] Before the rubbing process. [b] After the rubbing process.

generated from the rigid PI **7a** film could result from the steric interaction between the LC molecules and the straight units (stick out of the substrate surface of the PIs). In the previous study, Seo et al. also reported that the high pretilt angle of those materials often includes some fluorinated groups that tend to stick out of the surface of the PIs.[4d,e] PI **8a** and **8g** also had high pretilt angles (above 88°) after the rubbing process (Table 5). This is attributed to the fact that **8a** and **8g** are similar in conformation to **7a**. The two planes on both sides of the ether linkage are near orthogonal on the **8a** and **8g** PIs (inter-ring torsion angle 84° obtained from single crystal data of compound **5**). This means that the conformations of **8a** and **8g** also produced the alternative flat-straight structures, thereby generating the homeotropical alignment. These results suggest that the alternative flat-straight structures play a very import role in generating the LC pretilt angle. However, for PIs **7b**−**7f**, the pretilt angle lied in the range of a few degrees. The low pretilt angles are attributed to the fact that these PIs (**7b**−**7d**,**7f**) derived from the kink anhydrides, which induce chain distortion and increase conformational freedom, thereby destroying the out-of-plane orientation of the PIs (**7b**−**7d**,**7f**). Unexpectedly, **7e** derived from the rigid and linear BPDA exhibited a low pretilt angle. The exact mechanism of the low pretilt angle on **7e** is not yet clear. A possible reason for the low pretilt angle was that PMDA and NTDA molecules are smaller than BPDA. Therefore, the distance between the straight unit and the adjacent straight unit on the same chain for PI **7e** was longer than that for **7a**. The distances on the **7e** PIs seem to be too long to allow for an effective interaction with the aligned LC molecules, which leads to the low pretilt angles. Similar low pretilt angles were also generated in **8b**−**8f** PI alignment films. The low pretilt angles of **8b**−**8f** were similar in reason to those of **7b**−**7f**. These studies clearly confirmed that the PI alignment layers containing out-of-plane units can generate a high pretilt angle. The high pretilt angle can be achieved using the rigid PI alignment layers. Even though this work provides firm evidence of the high pretilt angle of PI films containing only short side groups, it is clear that further work is needed to correlate the molecular-scaled orientation of PI with the LC.

Conclusions

Two series of PIs that contain asymmetric di-*tert*-butyl pendent groups have been designed and synthesized for achieving high pretilt angle alignment layers. After mechanical rubbing at room temperature, PIs **7a**, **8a**, and **8g** had high pretilt angles of 87.9 to 88.7°. The pretilt angles of **8a** and **8g** were found to remain above 88° after annealing at 65 °C for 72 h. The unusually high pretilt angles were predominantly governed by their flat-straight structures. These studies clearly confirmed that the PI alignment layers that contain out-of-plane units can generate high pretilt angles. Owing to the low hydrophilicity and polarity of the *tert*-butyl and trifluoromethyl groups, the merits of new **7** and **8** series PIs were low dielectric constants and low moisture absorptions. The introduction of asymmetric *tert*-butyl and trifluoromethyl groups caused the decreased

intermolecular force between the polymer chains; therefore, the **7** and **8** PIs had excellent solubility. The **8a** and **8g** PIs derived from the very rigid PMDA and NTDA were soluble in NMP, DMAc, *m*-cresol, and THF. The soluble **8g** derived from the very rigid NTDA had a very high T_g (456 °C).

Acknowledgment. We appreciate the financial support provided by the National Science Council through Project NSC.

Supporting Information Available: Pretilt angles of **7a**, **8a**, and **8g** cells after the rubbing process. This material is available free of charge via the Internet at http://pubs.acs.org.

References and Notes

(1) Berreman, D. W. *Phys. Rev. Lett.* **1972**, *28*, 1683.
(2) Geary, J. M.; Gooby, J. W.; Kmetz, A. R.; Patel, J. S. *J. Appl. Phys.* **1987**, *62*, 4100.
(3) Toney, M. F.; Russel, T. P.; Logan, J. A.; Kikuchi, H.; Sands, J. M.; Kumar, S. K. *Nature* **1995**, *374*, 709.
(4) (a) Seo, D. S.; Kobayashi, S.; Nishikawa, M. *Appl. Phys. Lett.* **1992**, *61*, 2392. (b) Seo, D. S. *J. Appl. Phys.* **1999**, *86*, 3594. (c) Sugiyama, T.; Kumiyasu, S.; Seo, D.; Fukuro, H.; Kobayashi, S. *Jpn. J. Appl. Phys., Part 1* **1990**, *29*, 2045. (d) Seo, D. S.; Kobayashi, S. *Liq. Cryst.* **2000**, *27*, 883. (e) Nishikawa, M. *Polym. Adv. Technol.* **2000**, *11*, 404. (f) Nishikawa, M.; Taheri, B.; West, J. L. *Appl. Phys. Lett.* **1998**, *72*, 2403.
(5) Feller, M. B.; Chen, W.; Shen, Y. R. *Phys. Rev. A* **1993**, *43*, 6778.
(6) Wei, X.; Zhuang, X.; Hong, S. C.; Goto, T.; Shen, Y. R. *Phys. Rev. Lett.* **1999**, *82*, 4256.
(7) Lee, K. W.; Paek, S. H.; Lien, A.; Durning, C.; Fukuro, H. *Macromolecules* **1996**, *29*, 8894.
(8) (a) Kim, Y. B.; Ban, B. S. *Liq. Cryst.* **1999**, *26*, 1579. (b) Ban, B. S.; Rim, Y. N.; Kim, Y. B. *Liq. Cryst.* **2000**, *27*, 125.
(9) (a) Kim, S. I.; Pyo, S. M.; Ree, M.; Park, M.; Kim, Y. *Mol. Cryst. Liq. Cryst.* **1998**, *316*, 209. (b) Kim, S. I.; Ree, M.; Shin, T. J.; Jung, J. C. *J. Polym. Sci., Part A: Polym. Chem.* **1999**, *37*, 2909. (c) Chae, B.; Kim, S. B.; Lee, S. W.; Kim, S. I.; Choi, W.; Lee, B.; Ree, M.; Lee, K. H.; Jung, J. C. *Macromolecules* **2002**, *35*, 10119. (d) Park, J. H.; Sohn, B. H.; Jung, J. C.; Lee, S. W.; Ree, M. *J. Polym. Sci., Part A: Polym. Chem.* **2001**, *39*, 1800. (e) Kim, S. I.; Ree, M.; Shin, T. J.; Jung, J. C. *J. Polym. Sci., Part A: Polym. Chem.* **1999**, *37*, 2909. (f) Hahm, S. G.; Lee, T. J.; Chang, T.; Jung, J. C.; Zin, W. C.; Ree, M. *Macromolecules* **2006**, *39*, 5385.
(10) Samant, M. G.; Stohr, J.; Brown, H. R.; Russell, T. P.; Sands, J. M.; Kumar, S. K. *Macromolecules* **1996**, *29*, 8334.
(11) Mori, N.; Morimoto, M.; Nakamura, K. *Macromolecules* **1999**, *32*, 1488.
(12) (a) Ge, J. J.; Li, C. Y.; Xue, G.; Mann, I. K.; Zhang, D.; Wang, S. Y.; Harris, F. W.; Cheng, S. Z. D.; Hong, S. C.; Zhuang, X.; Shen, Y. R. *J. Am. Chem. Soc.* **2001**, *123*, 5768. (b) Wang, D. H.; Shen, Z.; Guo, M.; Cheng, S. Z. D.; Harris, F. W. *Macromolecules* **2007**, *40*, 889.
(13) Kikuchi, H.; Logan, J. A.; Yoon, D. Y. *J. Appl. Phys.* **1996**, *79*, 6811.
(14) Cai, C.; Lien, A.; Andry, P. S.; Chaudhari, P.; John, R. A.; Galligan, E. A.; Lacey, J. A.; Ifill, H.; Graham, W. S.; Allen, R. D. *Jpn. J. Appl. Phys.* **2001**, *40*, 6913.
(15) (a) Sakamoto, K.; Arafune, R.; Ito, N.; Ushioda, S.; Suzuki, Y.; Morokawa, S. *J. Appl. Phys.* **1996**, *80*, 431. (b) Arafune, R.; Sakamoto, K.; Ushioda, S. *Phys. Rev. E* **1998**, *58*, 5914.
(16) (a) Lee, Y. J.; Choi, J. G.; Song, I. K.; Oh, J. M.; Yi, M. H. *Polymer* **2006**, *47*, 1555. (b) Lee, Y. J.; Choi, J. G.; Song, I. K.; Oh, J. M.; Yi, M. H. *Polymer* **2006**, *47*, 1555.
(17) Wrighi, J.; Jorgensen, E. C. *J. Org. Chem.* **1968**, *33*, 1245.
(18) Tashiro, K.; Hama, H.; Yoshino, J. I.; Abe, Y.; Kitagawa, T.; Yabuki, K. *J. Polym. Sci., Part B: Polym. Phys.* **2001**, *39*, 1296.
(19) Owens, D. K. *J. Appl. Polym. Sci.* **1969**, *13*, 1741.

MA8022475